European Journal of Medicinal Chemistry Reports 6 (2022) 100069

HOSTED BY

Contents lists available at ScienceDirect

European Journal of Medicinal Chemistry Reports

journal homepage: www.editorialmanager.com/ejmcr/default.aspx

Synthesis of new *para*-aminobenzoic acid derivatives, *in vitro* biological evaluation and preclinical validation of DAB-2-28 as a therapeutic option for the treatment of bladder cancer

Yassine Oufqir [a,1], Laurie Fortin [a,1], Julie Girouard [a], Francis Cloutier [b], Maude Cloutier [b], Marie-France Leclerc [b], Denise Belgorosky [c], Ana María Eiján [c], Gervais Bérubé [b,*], Carlos Reyes-Moreno [a,**]

[a] *Laboratoire de Recherche en Oncologie et Immunobiologie (LROI) et Groupe de Recherche en Signalisation Cellulaire (GRSC), Département de Biologie Médicale, Université Du Québec à Trois-Rivières, Trois-Rivières, QC, Canada*

[b] *Laboratoire de Recherche en Chimie Médicinale (LRCM) et Groupe de Recherche en Signalisation Cellulaire (GRSC), Département de Chimie, Biochimie et Physique, Université Du Québec à Trois-Rivières, Trois-Rivières, QC, Canada*

[c] *Instituto de Oncología Ángel H. Roffo, Área de Investigación, Universidad de Buenos Aires, Buenos Aires, Argentina*

ARTICLE INFO

Keywords:
Aminobenzoic acid
Bladder cancer
Hydrazide derivatives
Inflammation
Interferon gamma
Interleukin 6
Macrophage
Nitric oxide
Tumor necrosis factor alpha

ABSTRACT

Chronic inflammation plays a crucial role in bladder cancer (BCa) development and progression. To offer a unique treatment opportunity for this type of cancer, a hydrazide derivative namely, **DAB-1**, was recently identified in our laboratory as a potential drug to target cancer-related inflammation. In preclinical models of murine BCa, this particular compound exhibited remarkable anticancer activities. Structurally, **DAB-1** is made from *para*-aminobenzoic acid and bears two different components, a maleimide and a hydrazide moieties, which are critical for its anti-inflammatory activity and its anticancer properties. In order to improve its biological potential, the hydrazide moiety was further modified to provide 3 s-generation molecules named, **DAB-2-28**, **DAB-2-31A,** and **DAB-2-31B**, and two third-generation molecules named, **DAB-3-27** and **DAB-3-33**. Data from *in vitro* studies revealed that, among the different DAB molecules under study, **DAB-2-28** has less cytotoxic activity with greater efficiency than **DAB-1** to inhibit the production of nitric oxide (NO) induced by the combination of IFNγ with TNFα, as well as the activation of pro-tumoral and pro-inflammatory signaling pathways IL6/STAT3 and TNFα/NFκB. Moreover, while **DAB-2-28** exhibited similar anti-inflammatory activity *in vivo* to **DAB-1** in a model of carrageenan-induced acute inflammation, it efficiently inhibited the expression of the enzymes iNOS and COX-2 induced by the combined activation of IFNγ with LPS in peritoneal macrophages. Notably, analysis of the growth kinetics of MB49-I tumors implanted subcutaneously in C57Bl/6 mice showed that **DAB-2-28** was more efficient to inhibit tumor development. In conclusion, this study provided preclinical proof-of-principle for **DAB-2-28** molecule in the treatment of BCa.

1. Introduction

There is a constant need to improve medicinal drugs, as well as, to investigate new treatment strategies against a variety of diseases including cancer. Recently, many researchers focus their attention on the role that chronic inflammation plays in the initiation and progression of cancers [1–4]. For example, breast and bladder cancers are closely linked to inflammation [5,6]. In the case of bladder cancer (BCa), substantial evidence suggests that chronic activation of inflammatory cells and signaling pathways within the tumor microenvironment contributes to the malignant transformation and the progression of cancer disease [6–9]. Among the major promoters of chronic inflammation, the transcription factors NFκB (nuclear factor kappa B) and STAT3 (signal

* Corresponding author.
** Corresponding author.
E-mail addresses: Yassine.Oufqir@uqtr.ca (Y. Oufqir), Laurie.Fortin2@uqtr.ca (L. Fortin), Julie.Girouard@uqtr.ca (J. Girouard), Francis.Cloutier2@uqtr.ca (F. Cloutier), Maude.Cloutier@inrs.ca (M. Cloutier), Marie-France.Leclerc@uqtr.ca (M.-F. Leclerc), d_belgo@hotmail.com (D. Belgorosky), anamariaeijan@gmail.com (A.M. Eiján), Gervais.Berube@uqtr.ca (G. Bérubé), Carlos.Reyes-Moreno@uqtr.ca (C. Reyes-Moreno).
[1] These authors contributed equally to this work.

https://doi.org/10.1016/j.ejmcr.2022.100069
Received 7 February 2022; Received in revised form 25 May 2022; Accepted 19 June 2022
Available online 23 June 2022

Abbreviation list

BCa	bladder cancer
Bacillus Calmette-Guerin	(BCG)
DAB	derivative of aminobenzoic acid
DMSO	dimethyl sulfoxide
IFNγ	interferon gamma
i.p	intraperitoneal
NO	nitric oxide
NFκB	nuclear factor kappa B
PBS	phosphate-buffered solution
STAT	signal transducer and activator of transcription
TNFα	tumor necrosis factor alpha

transducer and activator of transcription 3), are key tumor factors involved in the progression from carcinoma *in situ* to invasive BCa [6,10,11]. In particular, NFκB and STAT3 signaling act as critical downstream mediators of the primary inflammatory cytokines TNFα (tumor necrosis factor alpha) and IL6 (interleukin 6), which are released during malignant transformation and progression of BCa in a chronically inflammatory environment [6,10,11].

Expression of functional inducible nitric oxide synthase (iNOS) via NFκB activation in the tumor microenvironment is also important for the initiation of cancer-associated inflammation and stimulation of tumor growth, tumor angiogenesis and metastasis [12,13]. Sustained iNOS expression in tumor and tumor-associated macrophages is known to be responsible for continuous NO production, which can induce chemotherapy resistance and provide protection of tumor cells from apoptosis [14,15]. Conceivably, pharmacological inhibition of iNOS expression or activity was proposed as a therapeutic option to inhibit tumor growth [16,17].

We have recently synthesized a series of compounds named DABs, showing multiple biological properties: anti-inflammatory, anticancer and anti-metastatic activities [18,19]. This new technology takes advantage of a natural product, *para*-aminobenzoic acid (**PABA**) that is efficiently converted into the DAB molecules via only three to four chemical steps with excellent yields [18,19]. One of these PABA derivatives named **DAB-1** (Fig. 1) was thoroughly tested in our laboratory. It was discovered that the maleimide and hydrazide moieties that form the **DAB-1** molecule as well as the double bound in the maleimide moiety are all essential for its anti-inflammatory activity and its anticancer properties [18–22]. These studies are aimed to investigate **DAB-1** interaction with serum transport proteins, i.e. β-lactoglobulin and albumin [20], DNA [21], and transfer RNA [22] and we observed that drug-protein, drug-DNA and drug-transfer RNA conjugation occurs mainly by ionic contacts. Furthermore, tested in animal model, **DAB-1** displays significant anticancer activity reducing by 90% the development of a murine BCa without any signs of toxicity and by preventing metastasis to the lungs [8]. Overall, we revealed that this small molecule produces its biological action through inhibition of TNFα/NFκB and iNOS/NO pathways [8]. In order to improve its biological potential by producing **PABA** derivatives with reduced cytotoxic activity while having superior anti-inflammatory and anticancer activity than **DAB-1**, our laboratories have generated a series of 2nd and 3rd generation molecules by modifying its structure. These transformations led to hydrazide-based and hydrazone-based analogs for the 2nd and 3rd generation, respectively (Scheme 1). The therapeutic properties of these new molecules were evaluated *in vitro*, by regulating cell proliferation/viability, NO production, and activation of pro-inflammatory and pro-tumor signaling pathways IL6/STAT3 and TNFα/NFκB in murine MB49-I BCa cells. Their biological potential was also tested *in vivo*, by regulating inflammatory response in an acute inflammation mouse model, and tumor development in a preclinical model of murine BCa. This communication reports the synthesis and biological properties of these new anti-inflammatory compounds.

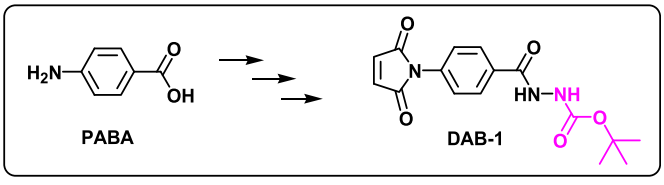

Fig. 1. The structure of **DAB-1** obtained from the natural product **PABA** [18,19].

2. Results and discussion

2.1. Chemistry

The starting material **DAB-1** was made from *para*-amino benzoic acid (PABA) with good overall yield following a three-step reaction sequence described in earlier studies [30]. Bearing in mind its unique biological properties as an anti-inflammatory, anticancer/antimetastatic agent, it was decided to further modify its structure with the aim of identifying a compound with enhanced properties. Therefore, this product was acylated with acetic anhydride and trimethylamine in dichloromethane at 20 °C for 30 min to yield two new closely related hydrazide analogs, **DAB-2-31A** (20%) and **DAB-2-31B** (trace) (Scheme 1). The latter can be obtained more efficiently (57% yield) upon treatment with a mixture of acetic anhydride and acetyl chloride at 60 °C for 2 h. Afterwards, **DAB-1** was reacted with trifluoroacetic acid (TFA) in dichloromethane removing the *tert*-butyloxycarbonyl group to yield **DAB-1.TFA** quantitatively. The crude product was reacted with acetic anhydride to yield **DAB-2-28**, a diacetylated hydrazide derivative with about 38% yield. **DAB-2-28**, **DAB-2-31A** and **DAB-2-31B** are classified as 2nd generation hydrazine-based analogs. **DAB-1-TFA** was also transformed into two new 3rd generation hydrazone-based derivatives **DAB-3-27** and **DAB-3-33**. Cinnamaldehyde and 2-hydroxy-3-methoxybenzaldehyde (or ortho-vanillin) were selected for that purpose. They are two naturally occurring products isolated from plants that are mainly used as flavoring agents and are innocuous to humans. Hence, **DAB-1.TFA** reacted with either cinnamaldehyde or 2-hydroxy-3-methoxy benzaldehyde in dichloromethane led to **DAB-3-27** and **DAB-3-33** with 76% and 89% yield, respectively. The new molecules were characterized by their respective infrared, proton and carbon nuclear magnetic resonance spectroscopy and by high-resolution mass analysis.

2.2. Evaluation of biological properties of second-generation DAB molecules

This set of experiments was planned to investigate whether 2nd generation DAB molecules exhibit reduced cytotoxic activity while having anti-inflammatory and anticancer activity superior to DAB-1. To evaluate the cytotoxic and anti-inflammatory activities of these new molecules, MB49-I cells were first pretreated for 60 min with the vehicle or with **DAB-1**, **DAB-2-28**, **DAB-2-31A** or **DAB -2-31B** at doses of 15 and 30 μM. Subsequently, the cells were washed and activated with IFNγ at 10 ng/mL and TNFα at 25 ng/mL. Cells and their corresponding supernatant were prepared to assess both the effect on cell viability with the MTT assay and NO production by the Griess reagent assay. In order to normalize the NO concentration and proliferation values obtained in each experiment, and taking in account this variability, we considered the NO production or proliferation of activated control cells as the reference point, assigning it the value of 100%. Thus, the NO production and cell proliferation/viability rates were presented as a percentage relative to the control.

The results reported in Fig. 2 show that **DAB-2-28** molecule significantly inhibits the production of NO more effectively than **DAB-1, DAB-**

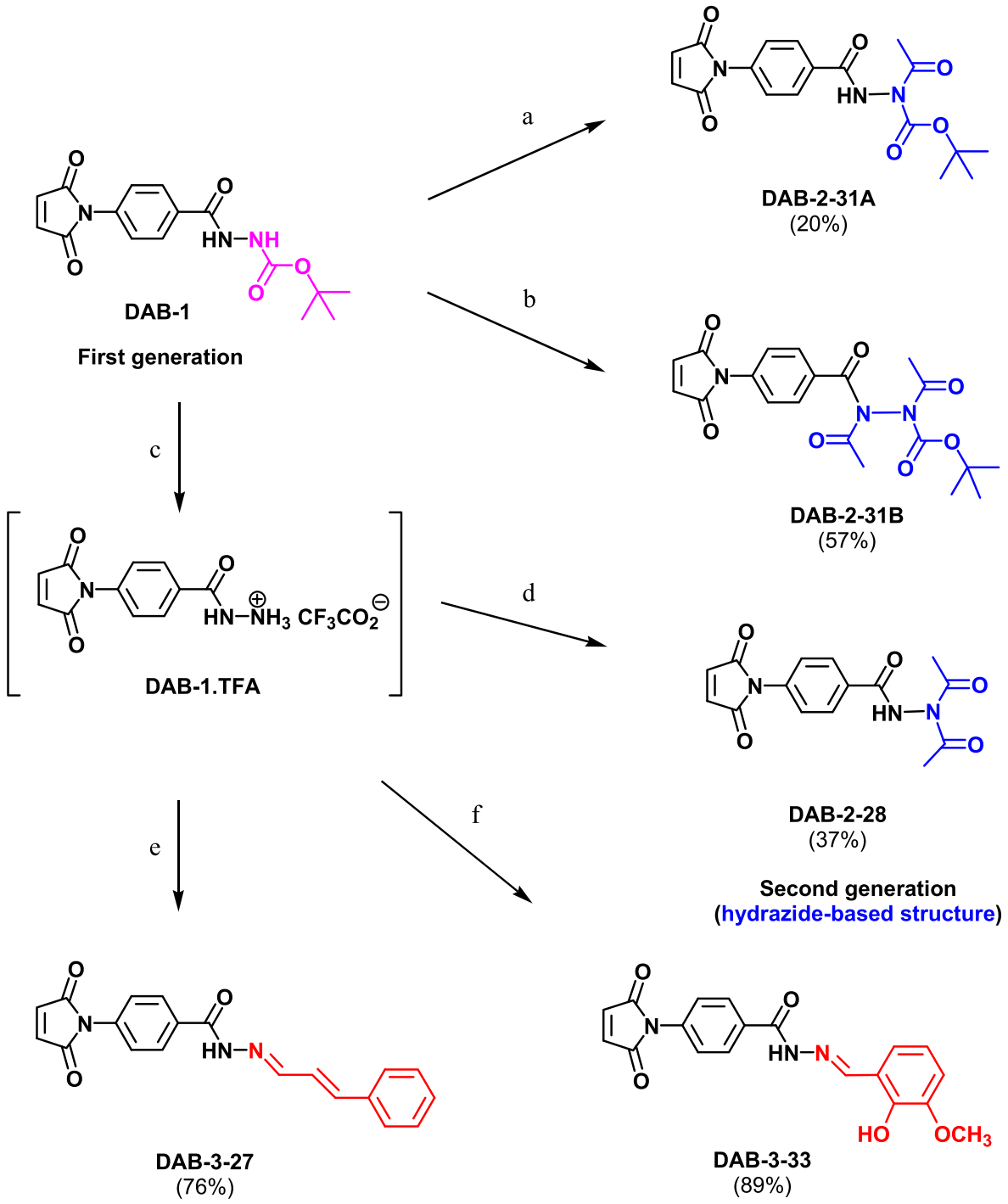

Scheme 1. Synthesis of second (blue) and third-generation (red) molecules from **DAB-1**. **Reagents and conditions:** a. Acetic anhydride, Et_3N, CH_2Cl_2, 20 °C, 0.5 h (**DAB-2-31A**, 20%); b. Acetic anhydride and acetyl chloride, Et_3N, CH_2Cl_2, 60 °C, 2 h (**DAB-2-31B**, 57%); c. TFA, CH_2Cl_2, 20 °C, 2 h (intermediate not isolated); d. Acetic anhydride, Et_3N, CH_2Cl_2, 40 °C, 0.5 h (**DAB-2-28**, 37%); e. Cinnamaldehyde, $NaHCO_3$, CH_2Cl_2 (**DAB-3-27**, 76%); f. 2-Hydroxy-3-methoxybenzaldehyde, $NaHCO_3$, CH_2Cl_2 (**DAB-3-33**, 89%).

2-31A or **DAB-2-31B** molecules with little or no effect on cell viability (Fig. 2a and c); the normalized NO inhibition relative to cell viability being 34% ± 3% at 15 μM (Figs. 2b) and 65% ± 5% at 30 μM (Fig. 2d). In contrast, the statistical analyzes indicated that, compared to **DAB-1**, **DAB-2-31A** and **DAB-2-31B** molecules both have similar negative effect on the rate of NO production as well as on cell viability (Fig. 2a and c), normalized NO inhibition relative to cell viability being on average 19% ± 2% at 15 μM (Figs. 2b) and 34% ± 4% at 30 μM (Fig. 2d).

The evaluation of the antitumor activity of **DAB-1** compared to 2nd generation DAB molecules was carried out by measuring the ability of these different molecules to inhibit the IL6/STAT3 (Fig. 3) and TNFα/NFκB signaling pathways (Fig. 4) in murine BCa MB49-I cells. The results

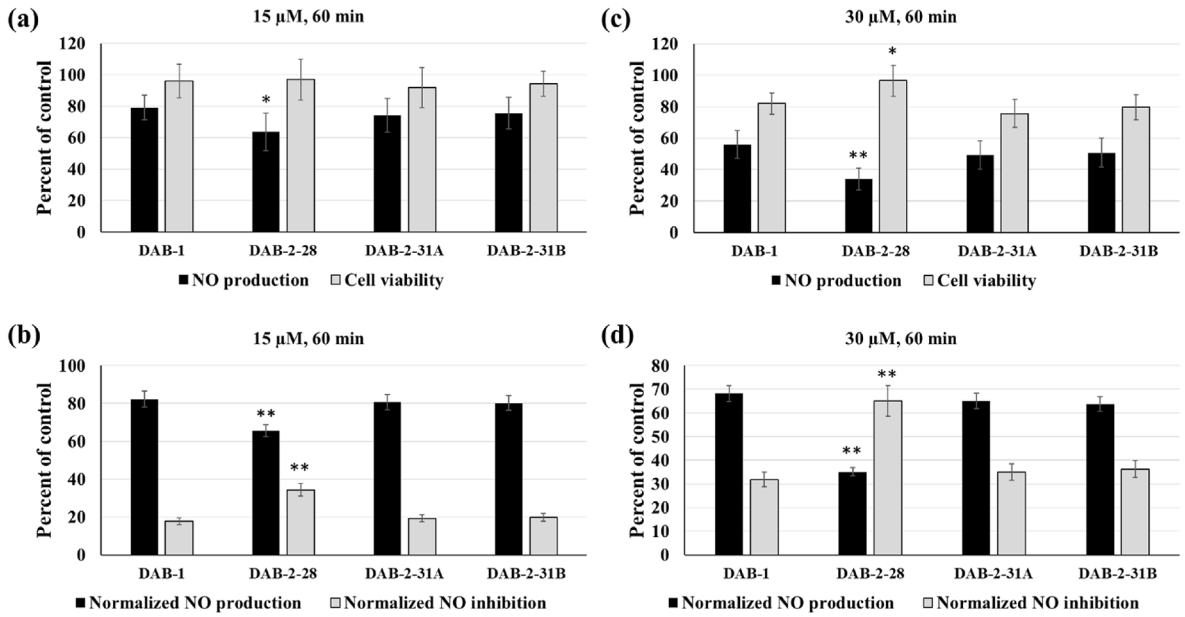

Fig. 2. Effects of DABs in cell viability and nitric oxide (NO) production in the murine BCa cell line MB49-I. Cells were pretreated with vehicle (DMSO) or **DAB-1**, **DAB-2-28, DAB-2-31A** and **DAB-2-31B** molecules at 15 µM and 30 µM for 60 min, then washed and activated with PBS or a combination of 10 ng/mL IFNγ and 25 ng/mL TNFα for 24 h. Cell viability and NO measurements were performed after 24 h of incubation. For cell viability and NO production, data are presented as percent of control **(a** and **c)** while NO production and NO inhibition rate were normalized to 100% viability **(b** and **d)**. $*p < 0.05$ and $**p < 0.01$ denote significant differences compared with **DAB-1** group.

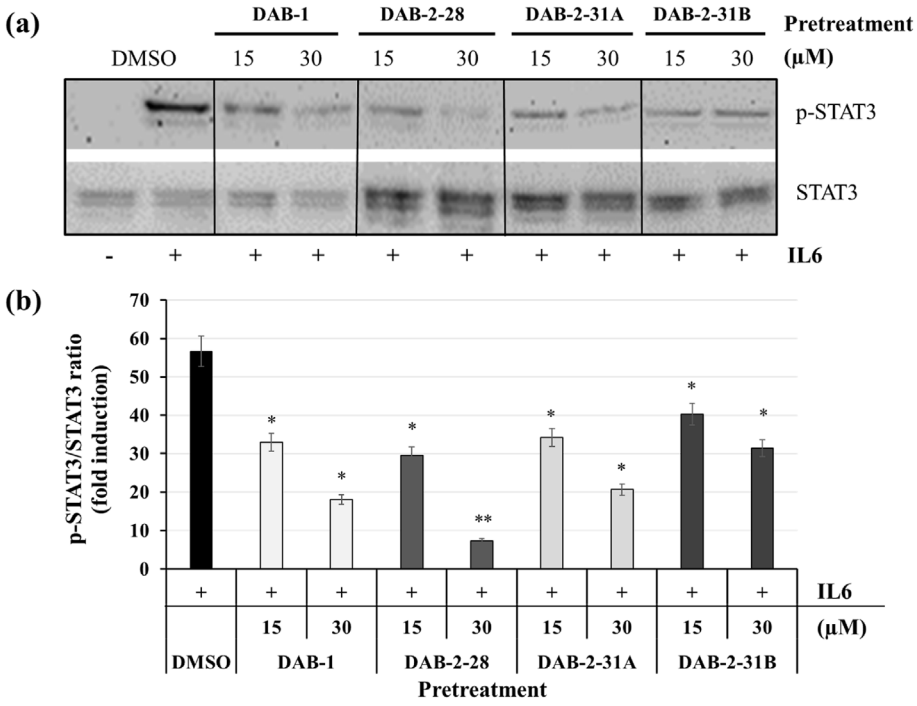

Fig. 3. Representative images **(a)** and graphical analysis **(b)** showing the immunodetection of phosphorylated STAT3 (p-STAT3) in MB49-I cells pretreated for 30 min with vehicle (DMSO) or **DAB-1**, **DAB-2-28, DAB-2-31A** and **DAB-2-31B** molecules at 15 and 30 µM, and then washed and recovered after 15 min of activation with 100 ng/mL IL6. The ratio of phosphorylated/unphosphorylated proteins was calculated from densitometric analysis of each sample to evaluate the relative activation of p-STAT3. $*p < 0.05$ and $**p < 0.01$ denote significant differences compared with vehicle control group.

reported in Fig. 3 show that the **DAB-2-28**, **DAB-2-31A** and **DAB-2-31B** molecules have a similar efficiency to that of **DAB-1** in inhibiting the level of STAT-3 protein phosphorylation (p-STAT3) induced by IL6. However, statistical analyzes indicate that the **DAB-2-28** molecule is more effective than **DAB-1**, **DAB-2-31A** and **DAB-2-31B** in inhibiting IL6-induced signaling at a dose of 30 µM (Fig. 3b). Finally, these results demonstrate that **DAB-2-31B** is the least effective DAB molecule in decreasing the level of p-STAT3 at doses of 15 and 30 µM (Fig. 3b).

Graphical and statistical analyzes of the phosphorylation level of IκB protein (*p*-IκB) in MB49-I cells pretreated with the vehicle or the DABs compounds demonstrate that **DAB-2-28** is more effective than **DAB-1**, **DAB-2-31A** and **DAB-2-31B** to inhibit TNFα-induced signaling even at doses of 15 and 30 µM (Fig. 4). Nonetheless, these results demonstrate that **DAB-2-31A** and **DAB-2-31B** are less effective than **DAB-1** and **DAB-2-28** in reducing the level of *p*-IκB protein induced by TNFα at a dose of 15 µM (Fig. 4b).

Taken together, these studies on the structure-activity relationship of **DAB-1** and 2nd generation DABs revealed that **DAB-2-28** has less

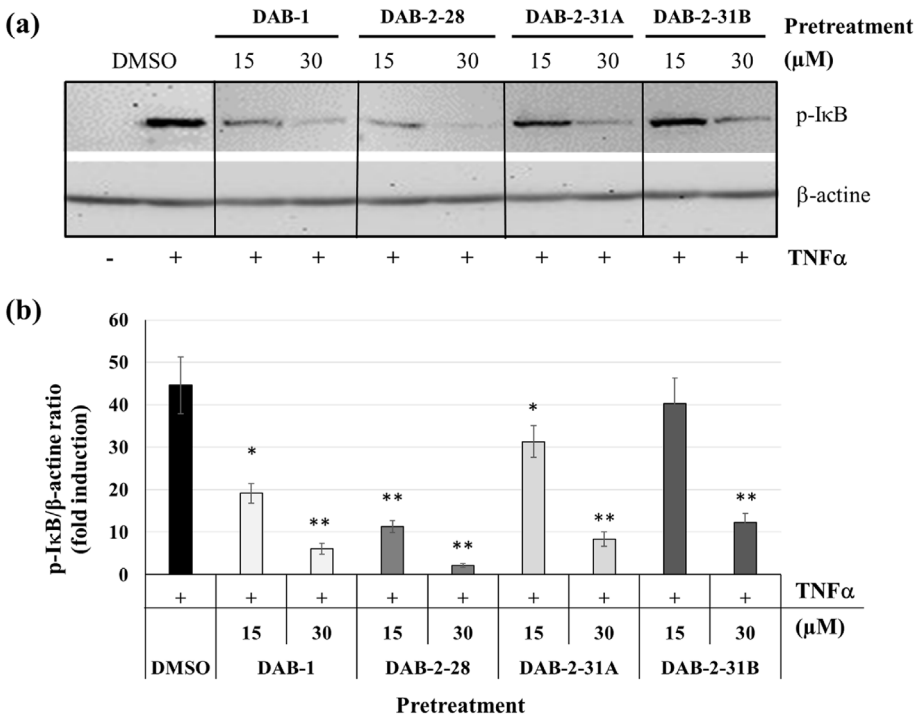

Fig. 4. Representative images **(a)** and graphical analysis **(b)** showing the immunodetection of phosphorylated IκB (*p*-IκB) in MB49-I cells pretreated for 30 min with vehicle (DMSO) or **DAB-1**, **DAB-2-28, DAB-2-31A** and **DAB-2-31B** molecules at 15 and 30 μM, and then washed and recovered after 5 min of activation with 25 ng/mL TNFα. The ratio of *p*-IκB/β-actin proteins was calculated from densitometric analysis of each sample to evaluate the relative activation of *p*-IκB. $*p < 0.05$ and $**p < 0.01$ denote significant differences compared with vehicle control group.

cytotoxic activity *in vitro* than the **DAB-1** molecule. Moreover, at low doses, **DAB-2 -28** is more effective than **DAB-1** in inhibiting both the production of NO induced by the IFNγ/TNFα combination and the pro-inflammatory and pro-tumor signaling pathways IL6/STAT3 and TNFα/NFκB in BCa MB49-I cells.

2.3. Evaluation of biological properties of third-generation DAB molecules

In this second structure-activity relationship study, we first compared the ability of two 3rd generation molecules, **DAB-3-27** and **DAB-3-33**, to regulate the activation of the IL6/STAT3 and TNFα/NFκB signaling pathways and the production of NO by MB49-I cells. In a first series of experiments, we compared the ability of **DAB-1**, **DAB-3-27** and **DAB-3-33** to regulate the activation of IL6/STAT3 (Fig. 5) and TNFα/NFκB signaling pathways (Fig. 6).

As reported in Fig. 5, the **DAB-3-27** molecule is less effective than the **DAB-1** and **DAB-3-33** molecules in inhibiting the level of IL6-induced p-STAT3. However, the statistical analyzes indicate that the **DAB-3-33** molecule is more effective than **DAB-1** in inhibiting the signaling induced by IL6 at doses of 20 and 30 μM (Fig. 5b).

Similar to the IL6/STAT3 signaling pathway, the results reported in Fig. 6 demonstrated that **DAB-3-27** is less effective than **DAB-1** and **DAB-3-33** in inhibiting TNFα-induced cell signaling. Still, the statistical analysis demonstrated that **DAB-3-33** is as effective as **DAB-1** in

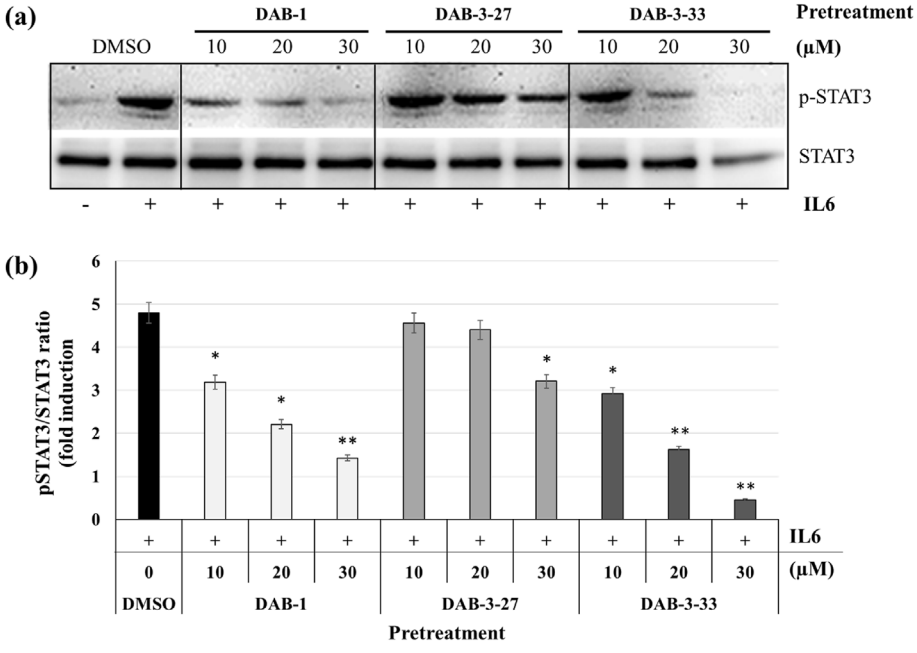

Fig. 5. Representative images **(a)** and graphical analysis **(b)** showing the immunodetection of phosphorylated STAT3 (p-STAT3) in MB49-I cells pretreated for 30 min with vehicle (DMSO) or **DAB-1**, **DAB-3-27,** and **DAB-3-33** molecules at 10, 20 and 30 μM, and then washed and recovered after 15 min of activation with 100 ng/mL IL6. The ratio of p-STAT3/STAT3 proteins was calculated from densitometric analysis of each sample to evaluate the relative activation of p-STAT3. $*p < 0.05$ and $**p < 0.01$ denote significant differences compared with vehicle control group.

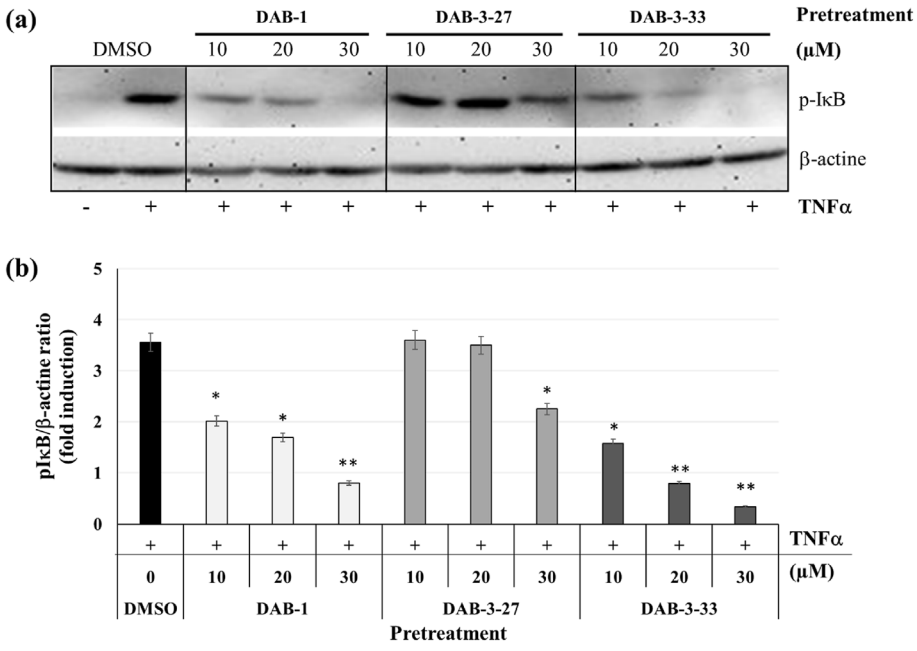

Fig. 6. Representative images **(a)** and graphical analysis **(b)** showing the immunodetection of phosphorylated IκB (*p*-IκB) in MB49-I cells pretreated for 30 min with vehicle (DMSO) or **DAB-1**, **DAB-3-27,** and **DAB-3-33** molecules at 10, 20 and 30 μM, then washed and recovered after 5 min of activation with 25 ng/mL TNFα. The ratio of *p*-IκB/β-actin proteins was calculated from densitometric analysis of each sample to evaluate the relative activation of *p*-IκB. $*p < 0.05$ and $**p < 0.01$ denote significant differences compared with vehicle control group.

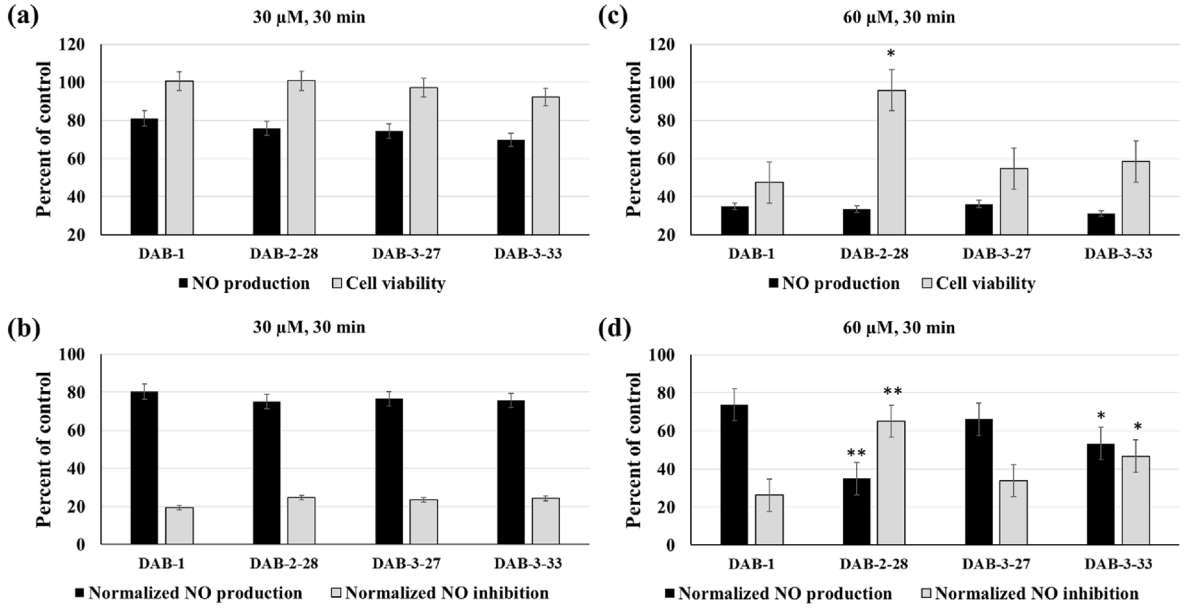

Fig. 7. Effects of DABs in cell viability and nitric oxide (NO) production. MB49-I cells were pretreated with DMSO (control) or **DAB-1**, **DAB-2-28**, **DAB-3-27,** and **DAB-3-33** molecules at 30 μM and 60 μM for 30 min, then washed and activated with PBS or a combination of 10 ng/mL IFNγ and 25 ng/mL TNFα for 24 h. Cell viability and NO measurements were performed after 24 h of incubation. For NO production and cell viability, data are presented as percent of control **(a** and **c)** while NO production and NO inhibition rate were normalized to 100% viability **(b** and **d)**. $*p < 0.05$ and $**p < 0.01$ denote significant differences compared with **DAB-1** group.

inhibiting the level of *p*-IκB in MB49-I cells at a dose of 30 μM (Fig. 6b). From these first studies, it is possible to conclude that the anticancer activity of **DAB-3-33** would be superior to that of **DAB-1**.

To determine if 3rd generation DAB molecules have superior anti-inflammatory activity while being less toxic than **DAB-1** or **DAB-2-28**, cells were pretreated for 30 min with vehicle, **DAB-1**, **DAB-2-28**, **DAB-3–27** or **DAB-3-33** at two different doses, 30 μM and 60 μM (Fig. 7). Cells were washed and then activated with 10 ng/mL IFNγ and 25 ng/mL TNFα for 24 h. Cells and their corresponding supernatant were prepared to assess both the effect on cell viability with the MTT assay and NO production by the Griess reagent assay. In order to normalize the NO concentration and proliferation values obtained in each experiment, and taking in account this variability, we considered the NO production or proliferation of activated control cells as the reference point, assigning it the value of 100%. Thus, the NO production and cell proliferation/viability rates were presented as a percentage relative to the control.

Results with DAB molecules pretreatment at a dose of 30 μM indicated that all molecules have a similar negative effect on the rate of NO production with little or no effect on cell viability (Fig. 7a), normalized NO inhibition relative to cell viability being on average 23% ± 3% (Fig. 7b). Nevertheless, data from cells pretreated at a dose of 60 μM indicated that all DAB molecules seem to have a similar negative effect on

the NO production, the production rate of NO being on average 34% ± 2% (Fig. 7c). However, statistical analysis demonstrates that compared to **DAB-2-28**, pretreatment with **DAB-1**, **DAB-2-27** and **DAB-3-33** molecules has a significant negative impact on cell viability, the average rate of cell viability relative to the control for these treatments being 54% ± 3% whereas the viability rate relative to the control is 96% in the cells pretreated with **DAB-2-28** (Fig. 7c). Thus, the inhibition rates of NO production normalized as relative to cell viability are 26%, 65%, 34% and 47% for cells pretreated with **DAB-1**, **DAB-2-28**, **DAB-2-27** and **DAB-3-33**, respectively (Fig. 7d). These results indicate that the down-regulation of 3rd generation DABs on NO production is due to an effect on the cell viability of MB49-I cells, **DAB-2-28** and **DAB-3-33** having very little effect on cell viability compared to **DAB-1** and **DAB-3-27**.

2.4. Evaluation of anti-inflammatory properties of selected DABs in a model of acute inflammation

The next objective of this study was to evaluate *in vivo* the anti-inflammatory activity of **DAB-1**, **DAB-2-28** and **DAB-3-33** in the model of acute inflammation induced by subcutaneous injection of carrageenan in CD-1 mice. This injection induces edema, inflammation and hyperalgesia at its injection site and therefore suitable for testing the anti-inflammatory and analgesic effects of anti-inflammatory molecules [23]. The process of formation of plantar edema induced with carrageenan is biphasic, the first phase between 2 h and 48 h involves the iNOS/NO system and the second phase, between 48 h and 72 h, the COX-2/prostaglandins system [23].

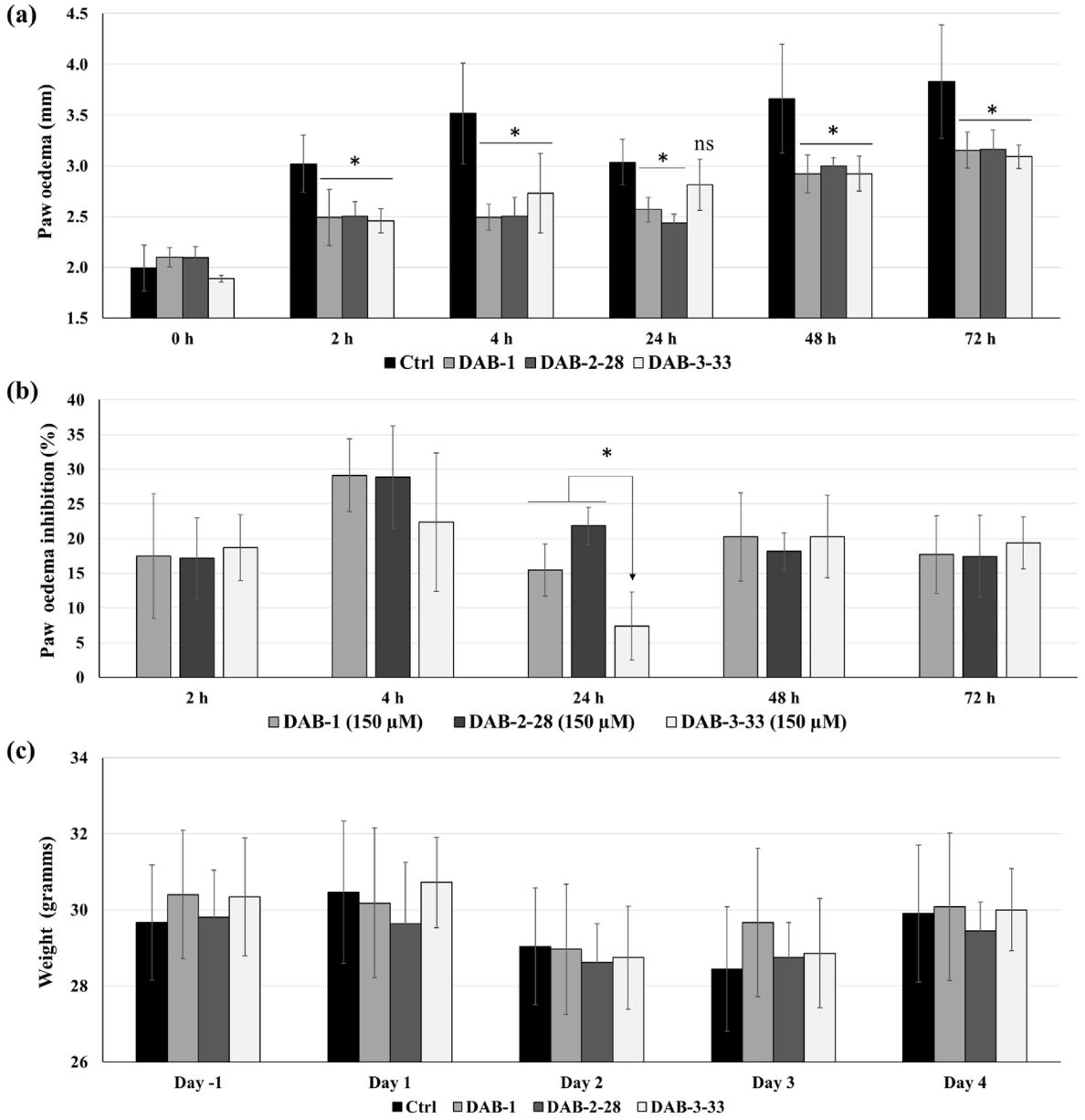

Fig. 8. Effects of **DAB-1, DAB-2-28** and **DAB-3-33** in an acute inflammation model. **(a)** Male CD-1 mice (5 mice/group) were injected intraperitoneally with **DAB-1**, **DAB-2-28** and **DAB-3-33** before (24 h and 1 h) and after (2 h, 4 h, 24 h, 36 h, 48 h and 60 h) injection of carrageenan. Carrageenan was injected on day 1 into the right paws of mice. Paw thickness (edema) measurements were recorded at t = 0 h and after sub-plantar carrageenan injection, at t = 2 h, t = 4 h, t = 24 h, t = 48 h and t = 72 h $*p < 0.05$ denote significant differences compared with vehicle control group. **(b)** The effect of DABs on carrageenan-induced inflammation was expressed as percent inhibition on the induction of intraplantar edema. $*p < 0.05$ denote significant differences compared with **DAB-1** and **DAB-2-28** groups. **(c)** Mouse weight was measured on day 1, day 1, day 2, day 3 and day 4 of the experiment.

The DABs molecules were injected intraperitoneally (i.p.), 24 h and 1 h before, and 2 h, 4 h, 24 h, 36 h, 48 h and 60 h after subplantar injection of carrageenan into the left hind paws of mice. Measurements of paw thickness (edema) were performed before (t = 0 h) and after (t = 2 h, 4 h, 24 h, 48 h and 72 h) injection of carrageenan. Fig. 8a indicated that the molecules **DAB-2-28** and **DAB-3-33** have anti-inflammatory effects similar to those of **DAB-1** during the first phase of the inflammatory process induced by carrageenan (i.e. to the iNOS/NO phase), both being effective at t = 2 h, t = 4 h and t = 24 h (Fig. 8a). In addition, the three DAB molecules are also effective in reducing subplantar edema at the second phase of the carrageenan-induced inflammatory process (i.e. at the COX-2/prostaglandins phase between 48 h and 72 h). However, statistical analysis of data from paw edema inhibition rates indicated that compared to **DAB-1** and **DAB-2-28**, **DAB-3-33** exhibit less robust anti-inflammatory effect at t = 24 h, i.e. the end of the iNOS/NO phase of carrageenan-induced inflammatory process (Fig. 8b). As shown in Fig. 8c, repeated i.p. injections with DAB molecules had no effect on normal development of mice as the average of bodyweight gain was not significantly different between groups of mice throughout DAB treatments.

2.5. Effects of DABs on iNOS and COX-2 protein expression by peritoneal macrophages

Studies in the acute inflammation model in mice having demonstrated that the anti-inflammatory effects of DABs are biphasic and act as inhibitors of the iNOS/NO and COX-2/prostaglandin systems, *in vitro* studies were carried out to determine and compare the effects of DAB molecules on the expression of iNOS and COX-2. To do this, peritoneal macrophages were pretreated for 30 min with the vehicle, **DAB-1**, **DAB-2-28** or **DAB-3-33** at a dose of 30 μM, washed and then activated with 100 ng/mL LPS and 10 ng/mL IFNγ. After 24 h of cell activation, the protein expression levels of iNOS and COX-2 enzymes were evaluated by the Western blot method (Fig. 9).

Densitometry analysis reveals that in the peritoneal macrophages pretreated with the vehicle, activation with LPS and INFγ combination induces a strong increase in the expression of the iNOS and COX-2 enzymes and a significant decrease in their expression after pretreatment with the DAB molecules (Fig. 9a). In addition, the statistical analysis demonstrates that cell pretreatment with **DAB-1** and **DAB-3-33** molecules has a similar negative impact on the expression of the iNOS enzyme (88% versus 89%) whereas **DAB-1** was more effective than **DAB-3-33** in inhibiting COX-2 protein expression (69% versus 45%) (Fig. 9b). More noticeable, **DAB-2-28** is the only DAB molecule under study to completely inhibit MB49-I iNOS and COX-2 expression in response to LPS and INFγ. Subsequently, preclinical studies were undertaken to investigate the efficacy of molecular therapy with **DAB-2-28** on tumor growth of MB49-I cells implanted subcutaneously (ectopically) in C57Bl/6 mice.

2.6. Growth kinetics of ectopic MB49-I tumors in response to selected DABs

To investigate the *in vivo* efficacy of **DAB-1** and **DAB-2-28** against subcutaneous tumors originating from MB49-I cells, 30 tumor-bearing

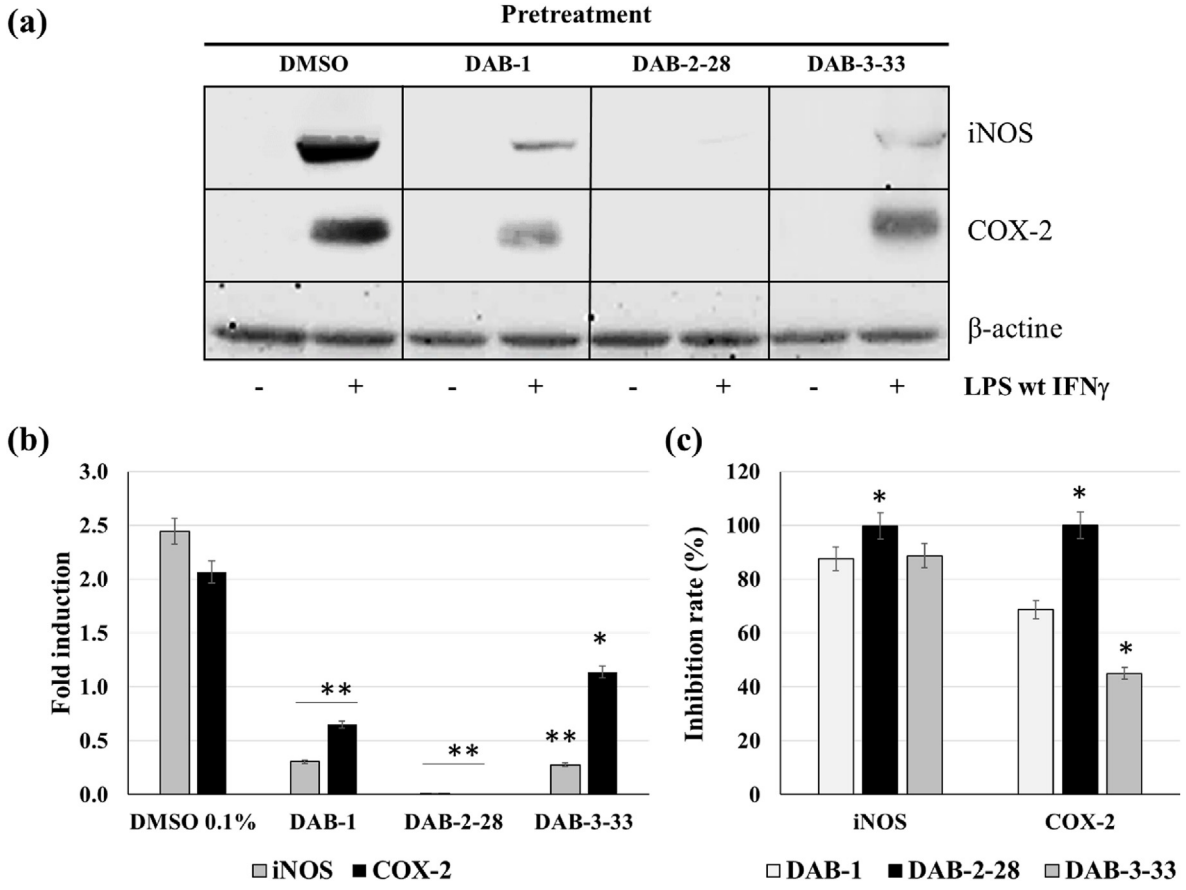

Fig. 9. Representative images **(a)** and graphical analysis **(b** and **c)** showing the influence of **DAB-1, DAB-2-28** and **DAB-3-33** on iNOS and COX-2 expression by peritoneal macrophages isolated from CD-1 mice. Pretreated cells with DABs at a dose of 30 μM for 30 min were washed and activated with LPS and IFNγ. Cell lysates were prepared from cell cultures after 24 h of incubation. Western blot assays were performed using specific antibodies. **(b)** The effect of DABs on protein expression was expressed as fold induction. $*p < 0.05$ and $**p < 0.01$ denote significant differences compared with vehicle control group. **(c)** Data is presented as percent inhibition of DABs on iNOS and COX-2 protein expression. $*p < 0.05$ denote significant differences compared with DAB-1 group.

C57Bl/6 mice were randomly divided to receive i.p. treatment with 100 µL of vehicle (0.1% DMSO in PBS; control group) or solutions of **DAB-1** at 150 µM and **DAB-2-28** at 150 µM. The molecules were injected 7 days following the inoculation of cancer cells. Analysis of tumor growth kinetics showed that tumors from mice in the control group grew significantly faster than tumors from mice treated with **DAB-1** and **DAB-2-28** (Fig. 10a). The mice were sacrificed on the 20th day after inoculation when mice in the control group have showed evidence of accelerated tumor progression and the tumor have reached their limit points. The results obtained on days 18 and 20 post-implantation showed that molecular therapy with **DAB-1** and **DAB-2-28** significantly reduce tumor growth compared to the control group. Indeed, at the end of the experiments, we found up to 3-fold and 4.5-fold decrease for **DAB-1** and **DAB-2-28** treated mice respectively, in comparison to the control group (Fig. 10a) without affecting mice body weight throughout the therapy (Fig. 10b).

3. Conclusion

DAB-1 was recently identified as a molecule showing anti-inflammatory and anticancer activity [8,19]. In this study, we prepared and characterized five analogs derived from **DAB-1** with the aim of improving the biological potential of this type of molecule. Two hydrazides were prepared by direct acylation of **DAB-1** leading to a mixture **DAB-2-31A** and **DAB-2-31-B**. Another acylated hydrazide derivative was synthesized through the intermediate **DAB-1.TFA** to give **DAB-2-28**. As well, the two new hydrazones were made still via **DAB-1-TFA** using cinnamaldehyde and 2-hydroxy-3-methoxybenzaldehyde to give **DAB-3-27** and **DAB-3-33**, respectively. The five molecules were tested *in vitro* for their biological potential including their anti-inflammatory and antiproliferative activity.

As a result, our different *in vitro, ex vivo* and *in vivo* studies about the structure-activity relationship of DABs revealed that **DAB-2-28** has a lower cytotoxic activity with a greater efficiency than **DAB-1** to

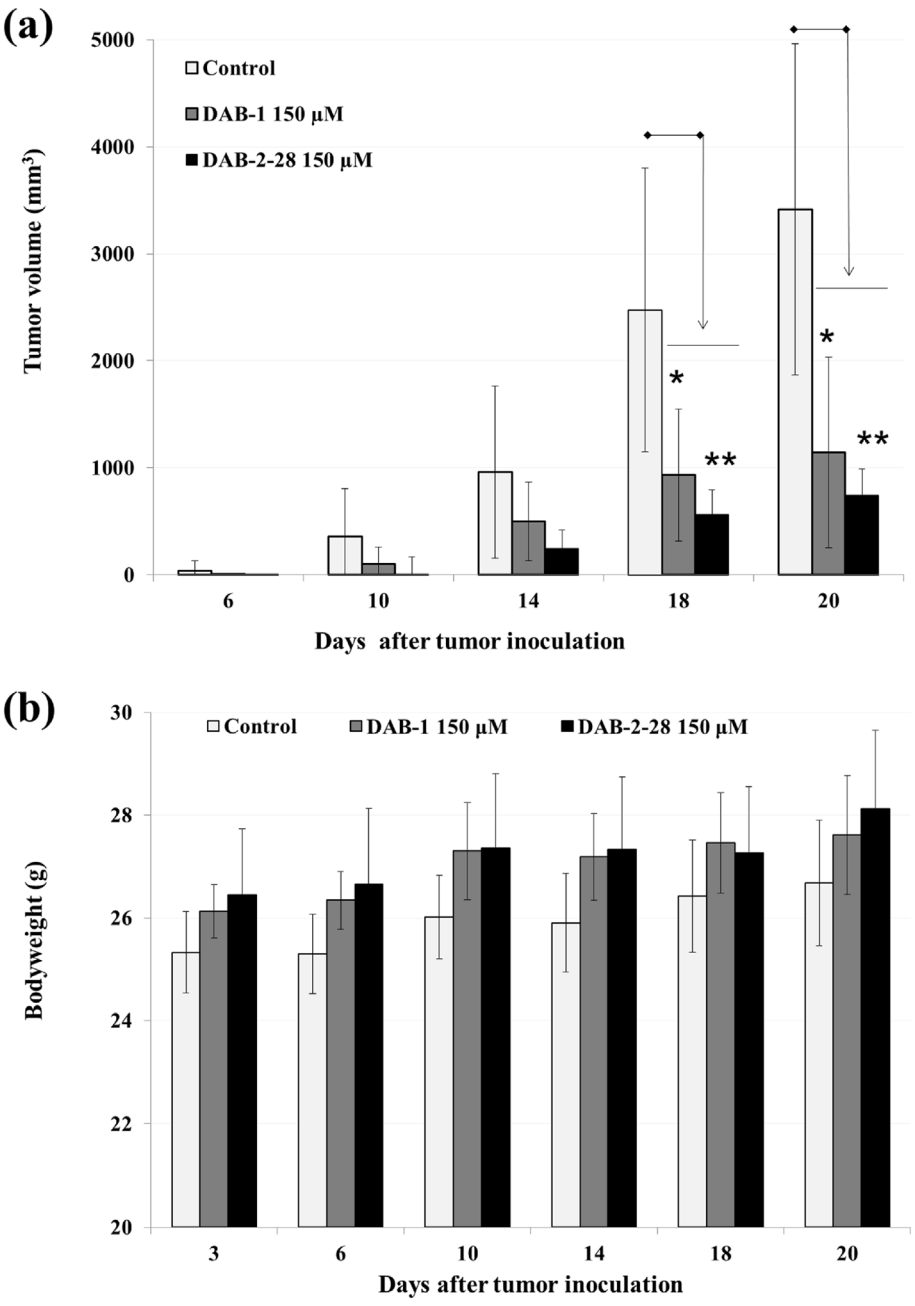

Fig. 10. Tumor growth of ectopic MB49-I tumors in response to **DAB-1** and **DAB-2-28** molecular therapy. **(a)** Graphical representation showing the effects of **DAB-1** and **DAB-2-28** on the development of MB49-I tumors subcutaneously implanted in male mice (n = 8); volume is expressed in mm^3 and correspond to the mean for each group of mice. **(b)** Body weight measurements in control (0.1% DMSO in PBS), **DAB-1** and **DAB-2-28** treated subgroups of male mice; data is expressed in grams and correspond to the mean for each group of mice. Error bars represent ±SEM. $*p < 0.05$ and $**p < 0.01$ denote significant differences compared with vehicle control group.

significantly inhibit: 1) the production of NO induced by the IFNγ/TNFα combination; 2) the IL6/STAT3 and TNFα/NFκB signaling pathways; 3) the expression of iNOS and COX-2 enzymes induced by the IFNγ/LPS combination; and 4) the growth of subcutaneous highly invasive MB49-I tumors. Hence, this simple compound might be of interest as a non-toxic anti-inflammatory derivative to investigate the role of inflammation in BCa and other cancers in the future. Further studies using an *in vivo* human model for BCa invasion and metastasis are currently underway to demonstrate the anticancer effects of this new anti-inflammatory molecule. Once completed, the results of these studies will be duly reported.

4. Experimental protocols

4.1. Chemistry

Anhydrous reactions were performed under an inert atmosphere of nitrogen. The starting material, reactant and solvents were obtained commercially and used as such or purified and dried by standard means [24]. Organic solutions were dried over magnesium sulfate ($MgSO_4$), filtered and evaporated on a rotary evaporator under reduced pressure. All reactions were monitored by UV fluorescence. Commercial TLC plates were Sigma T 6145 (polyester silica gel 60 Å, 0.25 mm). Flash column chromatography was performed according to the method of Still et al. on Merck grade 60 silica gel, 230–400 mesh [25]. All solvents used in chromatography were distilled prior to use.

The infrared spectra were taken on a Nicolet Impact 420 FT-IR spectrophotometer. Mass spectral assays were obtained using a MS model 6210, Agilent technology instrument. The high resolution mass spectra (HRMS) were obtained by TOF (time of flight) using ESI (electrospray ionization) using the positive mode (ESI+) (Université du Québec à Montréal and at Université Laval).

Nuclear magnetic resonance (NMR) spectra were recorded on a Varian 200 MHz NMR apparatus. Samples were dissolved in deuterochloroform ($CDCl_3$), deuteroacetone (acetone-d6) or deuterodimethylsulfoxide (DMSO-d_6) for data acquisition using tetramethylsilane or chloroform as internal standard (TMS, δ 0.0 ppm for ^{1}H NMR and $CDCl_3$ δ 77.0 ppm for ^{13}C NMR). Chemical shifts (δ) are expressed in parts per million (ppm), the coupling constants (J) are expressed in hertz (Hz). Multiplicities are described by the following abbreviations: s for singlet, d for doublet, t for triplet and m for multiplet, and bs for broad singlet.

4.1.1. Synthesis of *DAB-2-28, DAB-2-31A, DAB-2-31B, DAB-3-27* and *DAB-3-33*

*4.1.1.1. Synthesis of 4-(2,5-dioxo-2,5-dihydro-pyrrol-1-yl)-benzoic acid hydrazide trifluoroacetic acid salt (**DAB-1.TFA**).* A solution of **DAB-1** (106 mg, 0.32 mmol) dissolved in dichloromethane (1 mL) and trifluoroacetic acid (0.25 mL) was stirred at 20 °C for a period of 2 h. Afterwards, the solvent and excess trifluoroacetic acid were removed under vacuum to give compound **DAB-1.TFA** quantitatively. The crude product was used without purification for the synthesis of the diacetylated hydrazide product **DAB-2-28** as well as the two hydrazones derivatives **DAB-3-27** and **DAB-3-33**. The spectral data of the crude material corresponds to those reported in the literature [18]. **DAB-1.TFA**: IR (ν, cm^{-1}): 3500-2500 (CO_2H), 3277 (NH), 1710 (C═O); ^{1}H NMR (200 MHz, DMSO-d_6, δ ppm): 11.62 (br s, 1H, $NHNH_3^+CF_3CO_2^-$), 8.63 (br s, NH_3^+), 8.01 and 7.56 (2 × d, J = 8.5 Hz, 4H, aromatic), 7.24 (s, 2H, maleimide); ^{13}C NMR (50 MHz, DMSO-d_6, δ ppm): 169.6, 165.4, 135.5, 135.0, 129.4, 128.4, 126.5.

*4.1.1.2. Synthesis of N′,N′-diacetyl-4-(2,5-dioxo-2,5-dihydro-1H-pyrrol-1-yl)benzohydrazide (**DAB-2-28**).* This compound was obtained by a procedure described in a patent [18] with the following proportions of reagents and solvents; **DAB-1.TFA** (345 mg, 1.0 mmol), acetic anhydride (4.7 mL, 5.0 mmol), triethylamine (0.84 mL, 6 mmol), dichloromethane/DMSO (4 mL/0.2 mL). The mixture was stirred at 40 °C for 30 min. The crude material was purified immediately after the extraction to yield 38% of the final product. **DAB-2-28**. mp: Decomposition begins at 190 °C; IR (ν, cm^{-1}): 3194 (NH), 3093-3021 (C–H), 1701 (C═O), 1661 (C═O), 1607 (C═C); ^{1}H NMR (200 MHz, acetone-d6, δ ppm): 10.14 (s, 1H, NH), 8.09 and 7.61 (2 × d, J = 8.8 Hz, 4H, aromatic), 7.09 (s, 2H, maleimide), 2.41 (s, 6H, 2 × CH_3); ^{13}C NMR (50 MHz, acetone-d6, δ ppm): 171.1, 169.3, 166.0, 135.8, 134.7, 130.8, 128.2, 126.1, 24.2; ESI + HRMS: (M + H)+ calculated for $C_{15}H_{14}N_3O_5$ = 316.0928; found = 316.0945 and ESI + HRMS: (M + H -Ac)+ calculated for $C_{13}H_{12}N_3O_4$ = 275.08252; found = 275.0856.

*4.1.1.3. Synthesis of tert-butyl 1-acetyl-2-(4-(2,5-dioxo-2,5-dihydro-1H-pyrrol-1-yl)benzoyl)hydrazinecarboxylate (**DAB-2-31A**).* Acetic anhydride (71 μL, 0.75 mmol) and triethylamine (252 μL, 1.81 mmol) were added to a solution of **DAB-1** (100 mg, 0.30 mmol) dissolved in dichloromethane (3 mL). The mixture was stirred at 20 °C for 30 min. Afterwards, the organic phase was diluted with ethyl acetate (25 mL) directly into an extraction funnel. The organic phase was washed successively with a 5% sodium bicarbonate aqueous solution (10 mL), with a 10% sodium chloride aqueous solution (10 mL) and finally with water (20 mL). The organic phase was dried with anhydrous magnesium sulfate, filtered and evaporated to the crude material. The product was purified by flash column chromatography using a mixture of hexane/acetone (4/1) to give 22 mg (20%) of the desired material **DAB-2-31A**. It is noteworthy to say that a longer reaction time (2 h) gave higher yield of the desired material. However, some diacetylated product (**DAB-2-31B**) was also present as a side product. Spectral data for **DAB-2-31A**: IR (ν, cm^{-1}): 3286 (NH), 1753 (C═O), 1711 (C═O), 1652 (C═O); ^{1}H NMR (200 MHz, $CDCl_3$, δ ppm): 8.28 (s, 1H, NH), 7.90 and 7.50 (2 × d, J = 8.6 Hz, 4H, aromatic), 6.89 (s, 2H, maleimide), 2.61 (s, 3H, CH_3), 1.51 (s, 9H, 3 × CH_3); ^{13}C NMR (50 MHz, $CDCl_3$, δ ppm): 170.5, 168.9, 165.2, 151.0, 135.0, 134.4, 130.9, 128.3, 125.7, 84.8, 27.8, 25.5; ESI + HRMS: (M + Na)+ calculated for $C_{18}H_{19}N_3NaO_6$ = 396.1166; found = 396.1165 and ESI + HRMS: (M + H -*tert*-Boc)+ calculated for $C_{13}H_{12}N_3O_4$ = 274.0822; found = 274.0824.

*4.1.1.4. Synthesis of tert-butyl 1,2-diacetyl-2-(4-(2,5-dioxo-2,5-dihydro-1H-pyrrol-1-yl)benzoyl)hydrazinecarboxylate (**DAB-2-31B**).* Acetyl chloride (0.33 mL, 4.64 mmol), triethylamine (0.18 mL, 1.29 mmol) and 4-pyrrolidinopyridine (5 mg, 0.03 mmol) were added to a solution of **DAB-1** (100 mg, 0.30 mmol) dissolved in acetic anhydride (2 mL). The mixture was stirred at 60 °C for 2 h. Afterwards, the organic phase was diluted with ethyl acetate (25 mL) directly into an extraction funnel. The organic phase was washed successively with a 5% sodium bicarbonate aqueous solution (2 × 10 mL), with water (2 × 10 mL) and finally with brine (10 mL). The organic phase was dried with anhydrous magnesium sulfate, filtered and evaporated to the crude material. The product was purified by flash column chromatography using a mixture of hexane/acetone (4/1) to give 71.5 mg (57%) of the desired material **DAB-2-31-B**. mp: 57.0–59.5 °C; IR (ν, cm^{-1}): 3104-2940 (CH), 1712 (C═O), 1606 (C═C); ^{1}H NMR (200 MHz, acetone-d6, δ ppm): 7.72 and 7.56 (2 × d, J = 9.0 Hz, 4H, aromatic), 7.09 (s, 2H, maleimide), 2.46 and 2.39 (2 × s, 6H, 2 × CH_3), 1.52 (s, 9H, 3 × CH_3); ^{13}C NMR (50 MHz, acetone-d6, δ ppm): 170.2, 169.5, 169.2, 150.4, 135.3, 134.6, 133.0, 128.0, 125.6, 85.0, 27.0, 24.5, 23.3; ESI + HRMS: (M + Na)+ calculated for $C_{20}H_{21}N_3NaO_7$ = 438.1272; found = 438.1262.

*4.1.1.5. Synthesis of 4-(2,5-dioxo-2,5-dihydro-pyrrol-1-yl)-benzoic acid (3-phenyl-allylidene)-hydrazide (**DAB-3-27**).* The intermediate **DAB-1.TFA** was prepared as described above using the following quantities: derivative **DAB-1** (100 mg, 0.303 mmol), trifluoroacetic acid 250 μL, dichloromethane (1 mL). After evaporation of the reaction mixture, the intermediate **DAB-1.TFA** was redissolved in dichloromethane (2 mL) and

treated with cinnamaldehyde (2 eq., 0.303 mmol) and sodium bicarbonate (25.4 mg, 0.303 mmol). If necessary, dichloromethane (2–3 mL) was used to dissolve the aldehyde stuck to the reaction vessel wall. The reaction was stirred at room temperature for 12 h. Afterwards, hexane (1 mL) was added to the mixture allowing the hydrazone to completely precipitate. The solid was recovered on a fritted glass filter under vacuum, washed with dichloromethane (2 × 2 mL) and with water (3 × 2 mL) and the whole filter dried under vacuum. The solid was removed from the filter to give **DAB-3-27** with 76% yield as a pure product. mp: 220 °C; IR: (cm^{-1}) 3468 (NH), 1700 (C═O). ^{1}H NMR (DMSO-d_6, δ ppm): 11.80 (s, 1H, NH), 8.21 (s, 1H, CH═N), 7.97 and 7.49 (2 × d, J = 7.8 Hz, 4H, aromatic), 7.60 (d, J = 6.3 Hz, 2H, aromatic), 7.36 (m, 3H, aromatic), 7.18 (s, 2H, maleimide), 7.04 (m, 2H, aromatic); ^{13}C NMR (50 MHz, DMSO-d_6): δ (ppm) 170.09 (2), 162.91, 150.54, 139.79, 136.28, 135.26 (3), 134.90, 132.73, 129.31 (2), 128.70 (2), 127.57 (2), 126,.73 (2), 125.97; ESI + HRMS: (M + H)+ calculated for $C_{20}H_{16}N_3O_3$ = 346.1186; found = 346.1178.

4.1.1.6. Synthesis of 4-(2,5-dioxo-2,5-dihydro-pyrrol-1-yl)-benzoic acid (2-hydroxy-3-methoxy-benzylidene)-hydrazide ***(DAB-3-33)***. Following the same procedure as for the synthesis of **DAB-3-27** using 2-hydroxy-3-methoxybenzaldehyde (1.0 eq.) instead of cinnamaldehyde (2.0 eq.), the desired product **DAB-3-33** was obtained with 89% yield. mp: 136.2–140.2 °C. IR: (cm^{-1}) 3504 (NH), 3246 (OH), 2942 (CH_3), 1700 (C═O), 1372-1285 (Ar-O-CH_3); ^{1}H NMR (DMSO-d_6, δ ppm): 12.11 (s, 1H, NH), 10.90 (s, 1H, OH), 8.65 (s, 1H, CH═N), 8.01 and 7.53 (2 × d, J = 8.4 Hz, 4H, aromatic), 7.21 (s, 2H, maleimide), 7.15 (d, J = 7.4 Hz, 1H, aromatic), 7.05 (d, J = 7.4 Hz, 1H, aromatic), 6.88 (t, J = 7.9 Hz, 1H, aromatic), 3.80 (s, 3H, OCH_3); ^{13}C NMR (50 MHz, DMSO-d_6): δ (ppm) 170.02 (2), 16,263, 148.70, 148.41, 147.62, 135.32 (2), 135.12, 132.24, 128.74 (2), 126.76 (2), 121.18, 119.52, 119.39, 114.29, 56.27; ESI + HRMS: (M + H)+ calculated for $C_{19}H_{16}N_3O_5$ = 366.1084; found = 366.1075.

4.2. Biological evaluation

4.2.1. Cell culture

Biological assays were performed using the murine BCa cell line MB49-I, which is a highly invasive and tumorigenic BCa cell model that was developed by successive *in vivo* passages of MB49 primary tumors [26]. The cells were maintained in RPMI medium supplemented with 10% heat-inactivated fetal bovine serum (FBS) and containing 1 mM sodium pyruvate, 10 mM 4-(2-hydroxyethyl)piperazine-1-ethanesulfonic acid (HEPES) and 50 μg/mL gentamycin. The cells were maintained at 37 °C in a moisture-saturated atmosphere containing 5% CO_2. Isolation and cell culture of mouse peritoneal macrophages was performed as previously described [8].

4.2.2. Measurement of cell viability/proliferation

MB49-I cells were seeded in 96-well plates (5 × 10^4 cells/well) and incubated for 24 h in 5% CO_2 at 37 °C. In initial experiments, the cells were treated with vehicle (0.1% DMSO in PBS) or DAB molecules at different concentrations for 30 min, washed twice, and then cultured for 24 h to measure cell viability/proliferation by MTT assay as previously described [8,19]. In a second series of experiments, MB49-I cells cells were pretreated for 30 min with vehicle (0.1% DMSO in PBS), or different concentrations of DAB molecules and then activated for a period of 24 h with the cytokines IFNγ (10 ng/mL) and TNFα (25 ng/mL) to simultaneously measure cell viability/proliferation and NO production.

4.2.3. Measurement of nitric oxide (NO) production

MB49-I cells were seeded in 96-well plates (5 × 10^4 cells/well) and incubated in 5% CO_2 at 37 °C. After 24 h of incubation, the cells were pretreated for 30 min with vehicle (0.1% DMSO in PBS), or different concentrations of DAB molecules and then activated to produce NO for a period of 24 h in response to the cytokines IFNγ (10 ng/mL) and TNFα (25 ng/mL). The quantitation of NO production was performed in cell culture supernatants using the Griess reagent method (Life Technologies; # G-7921), as previously described [8,19]. This method involves the detection of nitrite ions (NO_2^-) formed by the spontaneous oxidation of NO under physiological conditions.

4.2.4. Cell signaling studies and protein immunodetection

Intracellular signaling studies were carried out by immunodetection of proteins of interest, in particular those linked to the pro-inflammatory and pro-tumor signaling pathways IL6/STAT3 and TNFα/NFκB in murine MB49-I tumor cells [8,19]. To study the regulatory effect of different DAB molecules on cytokine-activated BCa cells, MB49-I cells (50 × 10^3 cells/well in 24-well plates) were pretreated for 30 min with the vehicle, **DAB-1** or 2nd or 3rd generation DAB molecules at different concentrations (10, 15, 20 or 30 μM). Subsequently, the cells were stimulated with vehicle (PBS), TNFα (25 ng/mL, 5 min) or IL6 (100 ng/mL, 15 min) in order to study the activation status of IκB and STAT3 proteins, respectively. A signaling study was also carried out to determine and compare the effects of DAB molecules on the expression of iNOS and COX-2 using peritoneal macrophages from CD-1 mice. In this series of experiments, peritoneal macrophages (50 × 10^3 cells/well) were pretreated with vehicle, **DAB-1**, **DAB-2-28** or **DAB-3-33** at 15 μM for 30 min, washed and then activated with PBS (control) or a combination of 100 ng/mL LPS with 10 ng/mL IFNγ for 24 h. At the end of the signaling studies, cell lysates were prepared and immunodetection of phospho-STAT3 (pSTAT3), STAT3, *p*-IκB, iNOS, COX-2 and β-actin was performed as described [7,8,19,27]. The antibodies against pSTAT3 (pY705; #9145), STAT3 (#4904), *p*-IκB (# 9246), iNOS (# 2977), and COX-2 (#12282) were purchased from Cell Signaling Technology (Danvers, MA) and β-actin (# A3854) was from Sigma Chemical Company (Oakville, Canada).

4.2.5. Acute inflammation study in mice

Influence of DAB molecules on acute inflammatory response was assessed *in vivo* using the carrageenan-induced paw edema model as described [23]. Briefly, twenty CD-1 mice were randomized into 4 groups (n = 5) of animals treated with intraperitoneal (i.p.) injections of 100 μL of vehicle (0.1% DMSO in PBS; group 1), **DAB-1** (150 μM; group 2), **DAB-2-28** (150 μM; group 3) and **DAB-3-33** (150 μM; group 4) 24 h and 1 h before administering carrageenan. Paw edema was induced in all animals by subplantar injection (50 μl) of carrageenan (1% v/v) into the paws of the left hind legs of mice. Then, the vehicle and the DAB molecules, at 150 μM, were administered at 2 h, 4 h, 24 h, 36 h, 48 h and 60 h after the subplantar injection of carrageenan. To verify the presence of edema, paw thickness was measured using a micrometer 1 h before and after carrageenan injection at times t = 2 h, t = 4 h, t = 24 h, t = 48 h and t = 72 h. The effect of DAB molecules in paw thickness relative to the control group was expressed as percent inhibition of paw edema. To evaluate the normal development of mice, the body weight of each animal was recorded at days 1, 1, 2, 3, and 4. This animal study was conducted in accordance with the rules of the animal care and use committee of the Université du Quebec à Trois-Rivières (Trois-Rivières, Canada).

4.2.6. Ectopic murine bladder cancer model

The ectopic (subcutaneous) model of BCa was developed as described [8,16,28]. Briefly, murine MB49-I BCa cells (5 × 10^4 in 100 μL PBS) were injected subcutaneously into the left flank of 4-week-old C57Bl/6 male mice. At day 4 post tumor implantation, when the tumor reached a size of approximately 50 mm^3, each group of mice (n = 8) were given i.p. injections of either 0.1% DMSO in PBS (group 1), **DAB-1** at 150 μM (group 2), or **DAB-2-28** at 150 μM (group 3). I.p. injections were repeated every 2–3 days for three weeks. Growth rates of the subcutaneous tumors were monitored by measuring the size of tumors every 3–4 days using a digital caliper. The volume of the tumor was calculated by the following formula: length x $(width)^2$ x 0.52. Mice were examined daily for signs of

tumor progression, including visible signs of tumor growth, apathy or weight loss (2–3 g overnight), and were sacrificed when any of these signs became apparent. To evaluate the normal development of mice, the body weight of each animal was recorded at days 3, 6, 10, 14, 18, and 20. Mice were sacrificed 21 days after inoculation of MB49-I cells. The animal care and use committee of the Université du Quebec à Trois-Rivières (Trois-Rivières, Canada) have approved all animal procedures.

4.2.7. Statistical analyses

Data obtained from *in vitro* experiments are presented as means ± SEM from at least three independent experiments performed in triplicate. In the preclinical model of BCa, difference between groups was evaluated by unpaired two-tailed Student's t-test or two-way ANOVA followed by Bonferonni post-test, as described [7,8,19,27]. Statistical differences were considered to be significant at a value of $p < 0.05$ ($^{*}p < 0.05$, $^{**}p < 0.01$).

Declaration of competing interest

The authors declare that they have no known competing financial interests or personal relationships that could have appeared to influence the work reported in this paper.

Acknowledgments

The authors thank the Cancer Research Society (CRS: number 22471) and the Canadian Institutes of Health Research for financial support (CIHR; number 392334). This work was also sponsored by a grant from Aligo Innovation (number 150923), and the "*Ministère de l'Économie et de l'Innovation*", Québec Government to C. Reyes-Moreno and G. Bérubé. Y. Oufqir obtained a M.Sc. scholarship from the CIHR. L. Fortin holds a M.Sc. scholarship from the Fonds de la Recherche en Santé du Québec (FRSQ).

Appendix A. Supplementary data

Supplementary data to this article can be found online at https://doi.org/10.1016/j.ejmcr.2022.100069.

References

[1] H. Zhao, L. Wu, G. Yan, Y. Chen, M. Zhou, Y. Wu, Y. Li, Inflammation and tumor progression: signaling pathways and targeted intervention, Signal Transduct. Targeted Ther. 6 (2021) 263.
[2] A.E.R. Kartikasari, C.S. Huertas, A. Mitchell, M. Plebanski, Tumor-induced inflammatory cytokines and the emerging diagnostic devices for cancer detection and prognosis, Front. Oncol. 11 (2021), 692142.
[3] S.Y. Zhang, X.Y. Song, Y. Li, L.L. Ye, Q. Zhou, W.B. Yang, Tumor-associated macrophages: a promising target for a cancer immunotherapeutic strategy, Pharmacol. Res. 161 (2020), 105111.
[4] Y. Hu, J. Xiang, L. Su, X. Tang, The regulation of nitric oxide in tumor progression and therapy, J. Int. Med. Res. 48 (2020), 300060520905985.
[5] D.N. Danforth, The role of chronic inflammation in the development of breast cancer, Cancers 13 (15) (2021) 3918.
[6] X. Sui, L. Lei, L. Chen, T. Xie, X. Li, Inflammatory microenvironment in the initiation and progression of bladder cancer, Oncotarget 8 (2017) 93279–93294.
[7] M. Dufresne, G. Dumas, E. Asselin, C. Carrier, M. Pouliot, C. Reyes-Moreno, Pro-inflammatory type-1 and anti-inflammatory type-2 macrophages differentially modulate cell survival and invasion of human bladder carcinoma T24 cells, Mol. Immunol. 48 (2011) 1556–1567.
[8] J. Girouard, D. Belgorosky, J. Hamelin-Morrissette, V. Boulanger, E. D'Orio, D. Ramla, R. Perron, L. Charpentier, C. Van Themsche, A.M. Eijan, G. Berube, C. Reyes-Moreno, Molecular therapy with derivatives of amino benzoic acid inhibits tumor growth and metastasis in murine models of bladder cancer through inhibition of TNFalpha/NFKappaB and iNOS/NO pathways, Biochem. Pharmacol. 176 (2020), 113778.
[9] X. Huang, T. Pan, L. Yan, T. Jin, R. Zhang, B. Chen, J. Feng, T. Duan, Y. Xiang, M. Zhang, X. Chen, Z. Yang, W. Zhang, X. Ding, T. Xie, X. Sui, The inflammatory microenvironment and the urinary microbiome in the initiation and progression of bladder cancer, Genes. Dis. 8 (2021) 781–797.
[10] D.B. Thompson, L.E. Siref, M.P. Feloney, R.J. Hauke, D.K. Agrawal, Immunological basis in the pathogenesis and treatment of bladder cancer, Expert Rev. Clin. Immunol. 11 (2015) 265–279.
[11] Z. Zhu, Z. Shen, C. Xu, Inflammatory pathways as promising targets to increase chemotherapy response in bladder cancer, 2012, Mediat. Inflamm. (2012), 528690.
[12] F. Vannini, K. Kashfi, N. Nath, The dual role of iNOS in cancer, Redox Biol. 6 (2015) 334–343.
[13] H. Cheng, L. Wang, M. Mollica, A.T. Re, S. Wu, L. Zuo, Nitric oxide in cancer metastasis, Cancer Lett. 353 (2014) 1–7.
[14] C. Perrotta, D. Cervia, I. Di Renzo, C. Moscheni, M.T. Bassi, L. Campana, C. Martelli, E. Catalani, M. Giovarelli, S. Zecchini, M. Coazzoli, A. Capobianco, L. Ottobrini, G. Lucignani, P. Rosa, P. Rovere-Querini, C. De Palma, E. Clementi, Nitric oxide generated by tumor-associated macrophages is responsible for cancer resistance to cisplatin and correlated with syntaxin 4 and acid sphingomyelinase inhibition, Front. Immunol. 9 (2018) 1186.
[15] D. Dávila-González, D.S. Choi, R.R. Rosato, S.M. Granados-Principal, J.G. Kuhn, W.F. Li, W. Qian, W. Chen, A.J. Kozielski, H. Wong, B. Dave, J.C. Chang, Pharmacological inhibition of NOS activates ASK1/JNK pathway augmenting docetaxel-mediated apoptosis in triple-negative breast cancer, Clin. Cancer Res. 24 (2018) 1152–1162.
[16] D. Belgorosky, Y. Langle, B. Prack Mc Cormick, L. Colombo, E. Sandes, A.M. Eijan, Inhibition of nitric oxide is a good therapeutic target for bladder tumors that express iNOS, Nitric Oxide 36 (2014) 11–18.
[17] A.W. Chung, K. Anand, A.C. Anselme, A.A. Chan, N. Gupta, L.A. Venta, M.R. Schwartz, W. Qian, Y. Xu, L. Zhang, J. Kuhn, T. Patel, A.A. Rodriguez, A. Belcheva, J. Darcourt, J. Ensor, E. Bernicker, P.Y. Pan, S.H. Chen, D.J. Lee, P.A. Niravath, J.C. Chang, A phase 1/2 clinical trial of the nitric oxide synthase inhibitor L-NMMA and taxane for treating chemoresistant triple-negative breast cancer, Sci. Transl. Med. 13 (2021), eabj5070.
[18] G. Bérubé, C. Reyes-Moreno, Aminobenzoic Acid Derivatives for Use as Anti-inflammatory Agents, Anti-metastatic Agents And/or Anticancer Agents, 2020. US patent No. 10,759,754.
[19] J. Hamelin-Morrissette, S. Cloutier, J. Girouard, D. Belgorosky, A.M. Eijan, J. Legault, C. Reyes-Moreno, G. Berube, Identification of an anti-inflammatory derivative with anti-cancer potential: the impact of each of its structural components on inflammatory responses in macrophages and bladder cancer cells, Eur. J. Med. Chem. 96 (2015) 259–268.
[20] P. Chanphai, F. Cloutier, Y. Oufqir, M.F. Leclerc, A.M. Eiján, C. Reyes-Moreno, G. Bérubé, H.A. Tajmir-Riahi, Biomolecular study and conjugation of two para-aminobenzoic acid derivatives with serum proteins: drug binding efficacy and protein structural analysis, J. Biomol. Struct. Dyn. 39 (2021) 79–90.
[21] P. Chanphai, F. Cloutier, C. Reyes-Moreno, G. Bérubé, H.A. Tajmir-Riahi, Binding efficacy of aminobenzoic acid derivatives with DNA duplex: drug binding sites and DNA structure and dynamics, J. Biomol. Struct. Dyn. 39 (2021) 2278–2283.
[22] P. Chanphai, F. Cloutier, C. Reyes-Moreno, G. Bérubé, H.A. Tajmir-Riahi, Locating the binding sites of two aminobenzoic acid derivatives on tRNA: drug binding efficacy and RNA structure, J. Biomol. Struct. Dyn. 40 (2022) 130–135.
[23] I. Posadas, M. Bucci, F. Roviezzo, A. Rossi, L. Parente, L. Sautebin, G. Cirino, Carrageenan-induced mouse paw oedema is biphasic, age-weight dependent and displays differential nitric oxide cyclooxygenase-2 expression, Br. J. Pharmacol. 142 (2004) 331–338.
[24] W.L.F. Armarego, Chapter 3 - purification of organic chemicals, in: W.L.F. Armarego (Ed.), Purification of Laboratory Chemicals, eighth ed., Butterworth-Heinemann, 2017, 95-634.
[25] W.C. Still, M. Kahn, A. Mitra, Rapid chromatographic technique for preparative separations with moderate resolution, J. Org. Chem. 43 (1978) 2923–2925.
[26] V.T. Fabris, C. Lodillinsky, M.B. Pampena, D. Belgorosky, C. Lanari, A.M. Eijan, Cytogenetic characterization of the murine bladder cancer model MB49 and the derived invasive line MB49-I, Cancer, For. Genet. 205 (2012) 168–176.
[27] G. Dumas, M. Dufresne, E. Asselin, J. Girouard, C. Carrier, C. Reyes-Moreno, CD40 pathway activation reveals dual function for macrophages in human endometrial cancer cell survival and invasion, Cancer Immunol. Immunother. 62 (2013) 273–283.
[28] C. Lodillinsky, V. Rodriguez, L. Vauthay, E. Sandes, A. Casabe, A.M. Eijan, Novel invasive orthotopic bladder cancer model with high cathepsin B activity resembling human bladder cancer, J. Urol. 182 (2009) 749–755.